Available online at www.sciencedirect.com
SCIENCE DIRECT®
PERGAMON
Acta Astronautica 54 (2004) 325–335
ACTA ASTRONAUTICA
www.elsevier.com/locate/actaastro

Numerical simulation of drop Marangoni migration under microgravity

Yanxing Wang[a], Xiyun Lu[a,b,*], Lixian Zhuang[a], Zemei Tang[b], Wenrui Hu[b]

[a] *Department of Modern Mechanics, University of Science and Technology of China, Hefei, Anhui 230026, People's Republic of China*
[b] *National Laboratory of Microgravity, Institute of Mechanics, Chinese Academy of Sciences, 100080 Beijing, People's Republic of China*

Received 5 December 2001; received in revised form 14 May 2002; accepted 5 March 2003

Abstract

Thermocapillary motion of a drop in a uniform temperature gradient is investigated numerically. The three-dimensional incompressible Navier–Stokes and energy equations are solved by the finite-element method. The front tracking technique is employed to describe the drop interface. To simplify the calculation, the drop shape is assumed to be a sphere. It has been verified that the assumption is reasonable under the microgravity environment. Some calculations have been performed to deal with the thermocapillary motion for the drops of different sizes. It has been verified that the calculated results are in good agreement with available experimental and numerical results.

1. Introduction

The motion of drops and bubbles in a fluid medium, in which a temperature gradient is imposed, is of fundamental importance in the processing of materials in the reduced gravity environment and other applications. The motion of liquid drops and gas bubbles driven by the temperature gradient is called thermocapillary migration or Marangoni migration. Since the pioneering work of Young et al. [1], who derived the mathematical formula for the migration velocity of a spherical drop in a constant temperature gradient at small Reynolds and Peclet numbers by omitting the inertia force and convective energy transport, some succeeding work in this field has been performed experimentally, theoretically and numerically [2–10].

The drop Marangoni migration process in the ground-based experiments is usually coupled with the drop buoyant migration, and the pure Marangoni migration process can only be performed in the microgravity environment. It has been found that the experimental results of the drop Marangoni migration agree well with the YGB model only for very small diameter drops, e.g., the drop diameter of 11 ± 1.5 μm [2]. However, the migration velocities for the large diameter drops, e.g., 0.69–2.38 mm [3], proved to be smaller than those predicted by the YGB model. Recently, Xie et al. [4] also performed an experimental

* Corresponding author. Department of Modern Mechanics, University of Science and Technology of China, Hefei, Anhui 230026, People's Republic of China. Tel.: +86-551-3601542; fax: +86-551-3606459.
E-mail address: xlu@ustc.edu.cn (X. Lu).

0094-5765/$ - see front matter © 2003 Elsevier Ltd. All rights reserved.
doi:10.1016/S0094-5765(03)00158-9

study of a drop Marangoni migration at intermediate Reynolds numbers in the microgravity environment. They found that the drop Marangoni migration velocity depends on the temperature gradient and the drop diameter, and is obviously smaller than that calculated by the YGB linear model. More experiments, in which the migration velocity of drop is affected by both gravity and thermocapillary effects, have been performed on the ground. It was found that Marangoni and gravity effects could be expressed separately rather than being coupled with each other, so far as both the size of the drop and temperature gradient were small [5,6].

Theoretical analyses have been taken to investigate the problem of steady migration of a drop in a medium subjected to a temperature gradient. In the limiting case of a gas bubble, which was analyzed by Balasubramaniam et al. [7], the thermal conductivity of the gas in the bubble is considered to be negligible. Subramanian [8,9] investigated the motion of a gas bubble, taking the effect of convective transport of energy as a small perturbation, and extended the analysis to the case of a fluid drop, which accounted for the transport process in both phases. Recently Balasubramaniam et al. [10] furthered their theoretical work to the migration of a drop in a uniform temperature gradient at large Marangoni numbers.

Some numerical simulations for the migration of drops and bubbles have also been performed. Szymczyk et al. [11,12] calculated the steady migration of a gas bubble, but only solved the exterior flow outside the gas bubble. Balasubramaniam et al. [13] performed numerical simulation for higher Reynolds number and found that the migration velocity was mainly influenced by the Marangoni number rather than the Reynolds number. Interestingly, Geng et al. [14] investigated numerically the asymmetric drop Marangoni migration at larger Reynolds numbers and found that the trajectory of the drop oscillated periodically due to the vortex shedding in the near wake. Comprehensive numerical simulations of the thermocapillary motion of deformable drop have been taken by Haj-Hariri et al. [15,16] and Nas [17]. Haj-Hariri et al. [16] calculated the three-dimensional thermocapillary motion of deformable drops at finite Reynolds and Marangoni numbers. Nas [17] performed two- and three-dimensional calculations for both single drop and multiple drops. Some qualitative differences between the results of Haj-Hariri et al. [16] and Nas [17] were indicated by Ma et al. [18] in their axisymmetric drop migration calculations.

In this paper, thermocapillary migration of a drop in a uniform temperature gradient under microgravity environment has been investigated numerically. The three-dimensional incompressible Naiver–Stokes equations and the energy equation are solved by use of a Galerkin finite-element method [19]. To deal with the drop interface, the front tracking technique [20,21] is employed to smooth the discontinuity at the interface into a continuous distribution within a few meshes. To authors knowledge, it is the first time to employ the finite-element method combined with the front tracking technique to deal with the thermocapillary migration of a drop in a temperature gradient. In the present study, we developed a reasonable and efficient code to calculate the thermocapillary migration of a drop driven by the temperature gradient. Some typical cases, investigated experimentally by Xie et al. [4] and Hahnel et al. [5], are calculated and compared with those experimental results, which confirms the reliability of the present approach.

2. Governing equations

Three-dimensional incompressible Navier–Stokes and energy equations are used to investigate the thermocapillary motion of a drop in a uniform temperature gradient, which read

$$\nabla \cdot \vec{u} = 0, \tag{1}$$

$$\frac{\partial \vec{u}}{\partial t} + \vec{u} \cdot \nabla \vec{u} = -\frac{1}{\rho} \nabla p + \upsilon \nabla^2 \vec{u}, \tag{2}$$

$$\frac{\partial T}{\partial t} + \vec{u} \cdot \nabla T = \kappa \nabla^2 T, \tag{3}$$

where ρ (=constant), p and T are the density, pressure and temperature, respectively, $\vec{u}$ represents the velocity vector, υ and κ denote, respectively, the kinematic viscosity and thermo-diffusivity.

In this paper, we use the subscripts 1 and 2 to represent the fluids external and internal to the drop interface, respectively. A reference velocity for the motion

of the drop is usually adopted as

$$U = \left|\frac{\mathrm{d}\sigma}{\mathrm{d}T}\right| \cdot |\nabla T| a/\mu_2, \tag{4}$$

where σ denotes the surface tension, μ_2 is the dynamic viscosity of the fluid inside the drop, and a represents the radius of the drop. By using the velocity U, the drop radius a, $\Delta T = |\nabla T_\infty| a$, ρ_2, ν_2 and κ_2 as reference quantities to non-dimensionalize equations (1)–(3), the non-dimensional equations are given as

$$\nabla \cdot \vec{u} = 0, \tag{5}$$

$$\frac{\partial \vec{u}}{\partial t} + \vec{u} \cdot \nabla \vec{u} = -\frac{1}{\rho} \nabla p + \nu \frac{1}{Re} \nabla^2 \vec{u}, \tag{6}$$

$$\frac{\partial T}{\partial t} + \vec{u} \cdot \nabla T = \kappa \frac{1}{Ma} \nabla^2 T, \tag{7}$$

where Re represents the Reynolds number defined as $Re = Ua/\nu_2$, Ma denotes the Marangoni number defined as $Ma = Re\,Pr = Ua/\kappa_2$. For convenience, the symbols $\vec{u}$, ρ, p, T, ν and κ in Eqs. (5)–(7) are still used as the corresponding non-dimensional ones.

The initial conditions in a laboratory reference frame (as shown in Fig. 1) are given as

$$u|_{t=0} = v|_{t=0} = w|_{t=0} = 0, \tag{8}$$

$$T|_{t=0} = T_0 + z|\nabla T_\infty|, \tag{9}$$

where u, v, w represent the velocity components in x, y, z directions, respectively, and T_0 is a reference temperature (here, taken to be the temperature at the center of drop at the initial time, i.e., $x = y = z = 0$, $t = 0$), which is set to zero in the present calculation.

In this calculation, we assume that the drop keeps its spherical shape all the way during the thermocapillary motion. As is well known that this assumption works perfectly in the microgravity environment and enables the calculation to be much simplified. In order to be compatible with this assumption, we impose the boundary conditions at the interface as

$$\vec{u}_1 = \vec{u}_2, \quad T_1 = T_2, \quad k_1 \frac{\partial T_1}{\partial n} = k_2 \frac{\partial T_2}{\partial n}, \tag{10a}$$

$$\varepsilon_{kil}\left[\mu_1\left(\frac{\partial u_{1i}}{\partial x_j} + \frac{\partial u_{1j}}{\partial x_i}\right) - \mu_2\left(\frac{\partial u_{2i}}{\partial x_j} + \frac{\partial u_{2j}}{\partial x_i}\right)\right] n_j n_l = \nabla_S \sigma, \tag{10b}$$

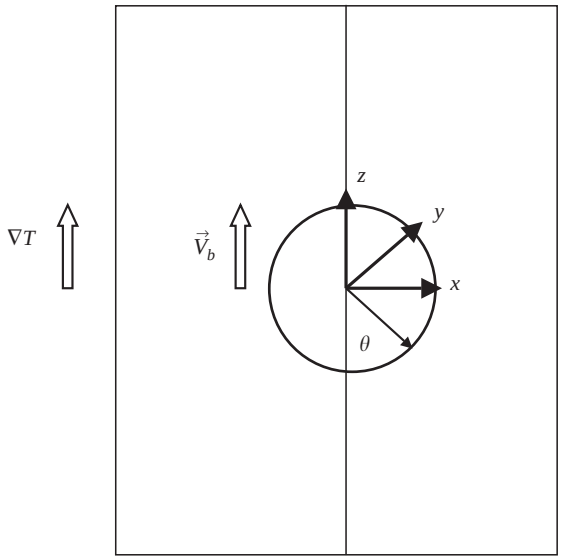

Fig. 1. Schematic of drop migration in a uniform temperature gradient.

where $\nabla_S \sigma$ is the gradient of surface tension, which is a vector tangential to the interface. The boundary condition for the normal stress on the interface is dropped here so as to meet the requirement of the no deformation assumption of spherical drop. Here, to meet the physical meaning clear, all quantities in the expressions of boundary condition at interface (10) are rewritten in the dimensional form and k is the thermo-conductivity. The boundary conditions at infinity are

$$\vec{u}_1 = 0 \quad \text{and} \quad T_\infty = T_0 + z|\nabla T_\infty|. \tag{11}$$

3. Numerical method

In the present calculation, the finite-element method is used to discretize the spatial derivatives in Eqs. (5)–(7). The velocity correction method is employed for the time advancing. The front-tracking technique [20,21] has been applied for the treatment of interface between fluid 1 and 2 in combination with the assumption of spherical configuration for the liquid drop. The advantages of this approach lie in that the computational grid system can be generated once for all by using the instantaneous inertial frame of reference and the flow field both external and internal to the

spherical drop can be calculated by solving the unified governing equations without interface boundary. The so-called "instantaneous inertial frame" is a frame fixed to the undisturbed field at infinity, but change its location with time such that its origin is always located at the center of the moving drop. To perform the calculation in the instantaneous inertial frame, the time derivatives in the Naiver–Stokes equations should be calculated in such a way that

$$\frac{\partial}{\partial t} = \left(\frac{\partial}{\partial t}\right)_{\mathrm{g}} - \vec{V}_b \cdot \nabla, \tag{12}$$

where $(\partial/\partial t)_{\mathrm{g}}$ is the time differentiation at a fixed grid point and $\vec{V}_b$ is the velocity of the moving drop as a whole.

In the front-tracking calculation, the interface is replaced by a transitional narrow zone, whose thickness is of the same order of magnitude as that of the mesh size. Across this narrow zone, the quantities vary smoothly by using the smooth approach suggested by Unverdi and Tryggvason [20]. In the present study, we simply use the following expressions to smooth the discontinuities at the interface. For example, the density ρ and kinematic viscosity v may be expressed by continuous functions like

$$\rho = \frac{\rho_1 - 1}{2}\sin\left(\frac{\pi s}{\varepsilon}\right) + \frac{\rho_1 + 1}{2}, \tag{13a}$$

$$v = \frac{v_1 - 1}{2}\sin\left(\frac{\pi s}{\varepsilon}\right) + \frac{v_1 + 1}{2}. \tag{13b}$$

Here, we set a spherical transitional zone of finite thickness ε at the instantaneous location of the drop interface, with the interface at the mid-way of the spherical zone. s $(-\varepsilon/2 \leqslant s \leqslant \varepsilon/2)$ is the radial displacement from the mid-way of the spherical zone. At the same time, the surface tension exerting of the interface is equivalently replaced by a volume force, $\vec{f}_v$, distributed continuously in the transitional zone [20].

To solve Eqs. (5)–(7), the velocity correction method proposed by Kovacs et al. [19] is used. Note that a volume force, $\vec{f}_v$, used to model the surface tension exerting on the interface based on the above analysis, must be added to the right-hand side of Eq. (6). Then the computational loop in the present study is described as follows:

Step 1: Calculation of the 'intermediate-velocity' field by using the explicit first-order Euler scheme for Eq. (6)

$$\vec{\tilde{u}} = \vec{u}^{\,n} - \Delta t\left[-v\frac{1}{Re}\nabla^2\vec{u}^{\,n} + (\vec{u}^{\,n}\cdot\nabla)\vec{u}^{\,n} - \vec{f}_v\right]. \tag{14}$$

Step 2: Solving the pressure Poisson equation in the form of

$$\nabla^2 p^{n+1} = \rho\frac{1}{\Delta t}\nabla\cdot\vec{\tilde{u}} \tag{15}$$

to meet the constraint of incompressible flow.

Step 3: Correction of the 'intermediate-velocity' field by adding the pressure terms missing in Eq. (14) to $\vec{\tilde{u}}$,

$$\vec{u}^{\,n+1} = \vec{\tilde{u}} - \Delta t\frac{1}{\rho}\nabla p^{n+1}. \tag{16}$$

Step 4: Calculation of the temperature field by the time-advancing scheme for Eq. (7)

$$T^{n+1} = T^n - \Delta t\left(\vec{u}\cdot\nabla T^n - \kappa\frac{1}{Ma}\nabla^2 T^n\right), \tag{17}$$

where the superscript n indicates the number of the time-step, and Δt is the time-step increment.

The finite-element discretization of Eqs. (14)–(17) is taken using the Galerkin weighted residual method via the following expansions in the piecewise polynomial basis functions:

$$\vec{u}(x,y,z,t) = \sum_{i=1}^{N}\vec{u}_i(t)\varphi_i(x,y,z), \tag{18a}$$

$$p(x,y,z,t) = \sum_{i=1}^{N} p_i(t)\varphi_i(x,y,z), \tag{18b}$$

$$T(x,y,z,t) = \sum_{i=1}^{N} T_i(t)\varphi_i(x,y,z), \tag{18c}$$

where N represents the node number for the velocity and pressure. The weak solution form of Eqs. (14)–(17) permits φ_i to be discontinuous in the first derivative and employs natural boundary conditions. Thus, $\varphi_i(x,y,z)$ is chosen to be a C^0 piecewise bilinear basis function defined in the isoparametric rectangular elements. Substituting (18) into the weak solution form of (14)–(17), we can reach the discretized system of

equations to be numerically solved. The details were described in our previous work for the viscous flow past a rigid sphere [22].

4. Results and discussion

Thermocapillary migration of drop in an unbounded immiscible liquid due to the presence of a temperature gradient in the z direction under microgravity environment, as shown schematically in Fig. 1, has been investigated numerically by using the finite-element method coupled with front-tracking technique. In this study, the grid number is $80 \times 80 \times 160$ in the x, y, and z directions (see Fig. 1), respectively, and the time step is 0.0002. Stretched transformations in the three directions are imposed to increase the grid resolution near the interface. A sketch of the grid generation is shown in Fig. 2.

Some results with different grid numbers and time steps are given below to show that our calculated results are independent of the grid number and time step. In one of our work [22], quantitative comparison has been performed to validate the present code. In addition, some typical cases which have been studied experimentally are calculated in the present calculation, and the physical parameters of the liquids used are the same as those in the experiments [4,5]. As an example, the physical parameters of liquid used by Xie et al. in their experiment [4] are listed in Table 1. The temperature gradient $|\nabla T_\infty|$ chosen in this calculation is 32°C/cm, following Xie et al. experiment [4], and 9.3°C/cm, following Hahnel et al. experiment [5]. Several drop sizes are listed in Table 2. Then the reference velocity in Eq. (4) can be determined based on the physical parameters of liquid, the temperature gradient and the drop size. Some comparisons between the calculated and experimental results to verify quantitatively the present calculation are taken as follows.

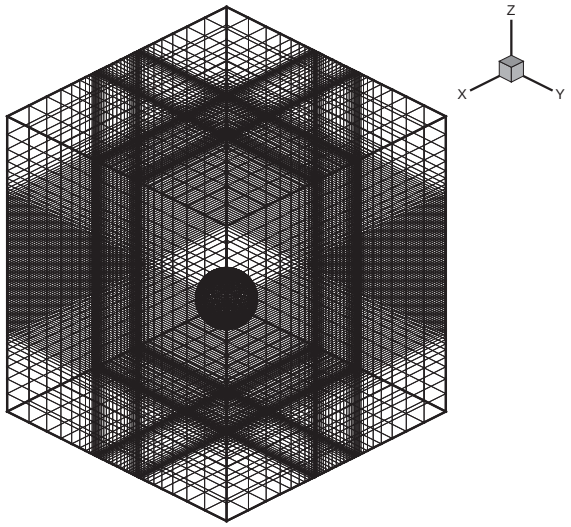

Fig. 2. Sketch of grid generation.

Table 1
Physical parameters of liquids used in experiment [4]

	Temperature (°C)	15
Drop liquid	Dynamic viscosity (dyn s/cm^2)	0.0509
	Thermal diffusivity (mW/m K)	112
	Density (g/cm^3)	0.919
	Thermal expansion coeff. (1/K)	0.00118
Mother liquid	Dynamic viscosity (dyn s/cm^2)	0.922
	Thermal diffusivity (mW/m K)	176
	Density (g/cm^3)	0.919
	Thermal expansion coeff. (1/K)	0.00081
	Interfacial tension (dyn/cm)	1.51
	$d\sigma/dT$ (dyn/cm K)	−0.0339

To depict the thermocapillary migration of the drop, the variations of the migration velocity with time for different drop diameters are shown in Fig. 3, where the velocity and time have been transformed to the dimensional values for comparing with experimental data [4]. At the beginning, the drop is accelerated from rest. Then the migration velocity approaches asymptotically to a constant value and the drop motion tends to a steady state. This behavior is consistent with the experimental observation [4]. It can be seen that the drop diameter is bigger, the migration velocity is larger. To examine the effect of the grid number and time step on the calculated results, the results calculated by the grid number $160 \times 160 \times 320$ and the time step 0.0001 (Condition-2) are also shown in Fig. 3.

The curves of migration velocity versus time, corresponding to the cases investigated experimentally by Hahnel et al. [5], are shown in Fig. 4, where the temperature gradient is smaller than that used in [4] and the sizes of drop are greater than those in [4].

Table 2
Comparison between the present calculated results and experimental data for the drop migration velocity

	∇T(°C/cm)	a(mm)	V_{exp}(mm/s)	V_{num}(mm/s)	$\lvert V_{num} - V_{exp}\rvert / V_{exp}$(%)
Drop shaft experiment [4]	32	3.77	0.77	0.833	8.18
		3.26	0.61	0.644	5.57
		2.59	0.45	0.426	5.33
Sounding rocket experiment [5]	9.3	2.38	4.12×10^{-2}	4.41×10^{-2}	7.04
		2.12	3.42×10^{-2}	3.67×10^{-2}	7.31
		1.98	3.36×10^{-2}	3.30×10^{-2}	1.79
		1.82	2.83×10^{-2}	2.84×10^{-2}	0.35
		1.74	2.50×10^{-2}	2.65×10^{-2}	6.00

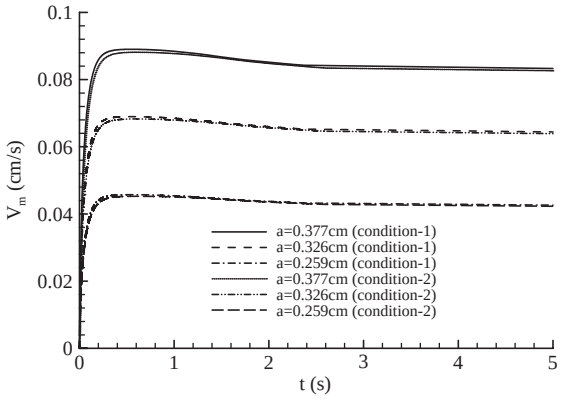

Fig. 3. Migration velocity evolution versus time for the experimental cases in Xie et al. [4]. Condition-1: grid number $80 \times 80 \times 160$ and time step 0.0002; Condition-2: grid number $160 \times 160 \times 320$ and time step 0.0001.

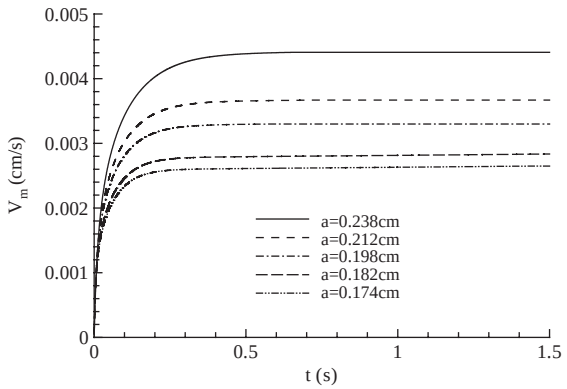

Fig. 4. Migration velocity evolution versus time for the experimental cases in Hahnel et al. [5].

The variations of the migration velocity (asymptotic value) with the drop diameter are given in Figs. 5 and 6. It can be seen that as the drop diameter increases, corresponding to increasing the Reynolds and Marangoni numbers, the migration velocity increases too. The experimental data [4,5] are also plotted in Figs. 5 and 6 to examine the present calculations. It is found that our calculated results are in good agreement with the experimental data. In addition, the comparisons between the present results and experimental values [4,5] confirm that the assumption of the spherical drop shape under microgravity environment is reasonable. The asymptotic velocity of drop migration calculated by Geng et al. [14] using the two-dimensional flow equations is also plotted in Fig. 5, which proves to be much larger than that of the spherical drops at the same size. This phenomenon can be explained as follows. Under the asymptotic steady flow state, the thermocapillary force caused by the surface tension in a temperature gradient is balanced by the viscous drag force. We can estimate the viscous drag force approximately by the Stokes formulae, which are $D = 6\pi\mu Ru$ and $D = 1.5\pi\mu Ru$ for the sphere and circular cylinder, respectively [23], here R representing the radius of the sphere and cylinder. This means that the resistance of the drop migration due to the fluid viscosity is much smaller for the circular cylinder of unit length than that for the sphere of the same size. On the other hand, the Marangoni driving force exerting on the sphere can

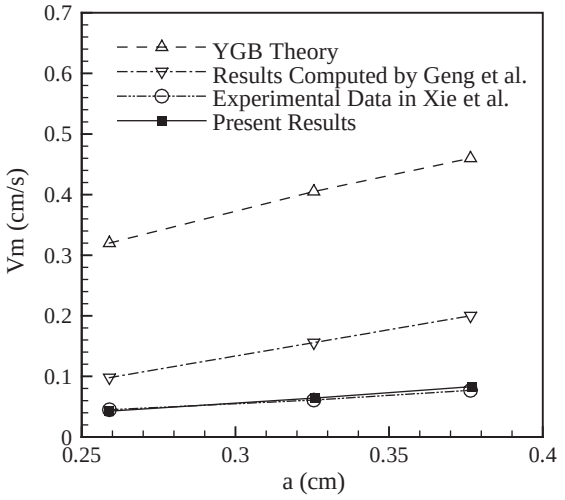

Fig. 5. Comparison among experimental data, numerical results, YGB linear theory and the present results for the asymptotic migration velocity.

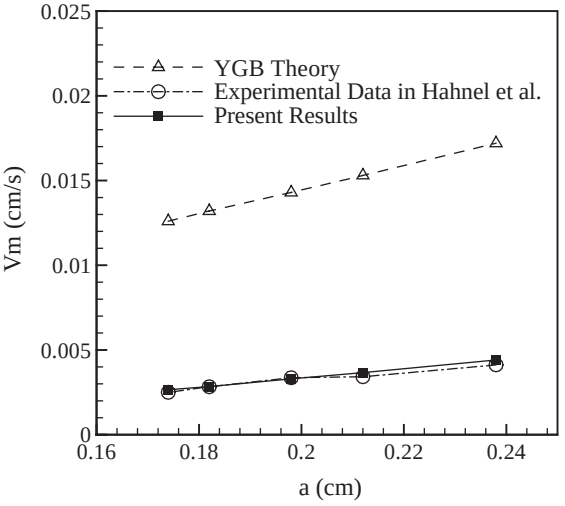

Fig. 6. Comparison among experimental data, YGB linear theory and the present results for the asymptotic migration velocity.

be estimated to be only slightly greater than that exerting on a cylinder of equal size. So, to balance the surface tension, the cylinder must move at a larger speed than that for a sphere of the same size. The curve of migration velocity predicted by the YGB linear model is also plotted in Figs. 5 and 6, which is even higher than those obtained by the calculations of Geng et al. [14]. Such discrepancy has been found in the previous work [3–6,14–18]. To quantitatively compare the calculated results and experimental data [4,5], the values of the migration velocity are listed in Table 2 for different drop diameters.

Although our calculation is a fully three-dimensional one, the calculated results prove to be axially symmetrical. So, we can express the flow field by the flow patterns in any meridian plane. The isotherms in the $x-z$ plane are shown in Fig. 7 for the three different drop diameters. The isotherms drawn in the figure are all equally spaced with dimensionless temperature increment of 0.2. Within the drop, the fluid near the front part of the drop is cooled by the heat convection. From the patterns for different drop diameters, it is found that the enhanced convection of heat with the increase of drop diameter results in the wrapping of the isotherms around the front of the drop. The surface temperature distributions are shown in Fig. 8. To enable the comparison between the temperature distributions for different drop diameters, the surface temperature shown in Fig. 8 are adjusted such that a zero value is set to the aft stagnation point of the drop. The surface temperature distributions indicate the decrease in the front part of the drop with increasing the drop diameter or increasing the Reynolds and Marangoni numbers. This behavior is consistent with the experimental and previous computational results [5,16,18].

The streamlines in the $x-z$ meridian plane, corresponding to the cases shown in Fig. 7, are illustrated in Fig. 9. Note that the drop diameters shown in Fig. 9 and in the following figures have been normalized to be of unit radius. Relative to the moving drop, the flow pattern within the drop exhibits recirculation bubble that is similar to the Hill's spherical vortex. Combining Figs. 9 and 7, we can see that the isotherms and the streamlines depict the thermal and fluid motion structures within and outside the drop, which is in good agreement with the calculated results of Haj-Hariri et al. [16] and Ma et al. [18]. The streamline patterns in an inertial laboratory reference frame are shown in Fig. 10. It is illustrated that those streamline patterns in Figs. 9 and 10 are very similar for different drop diameters, although obvious difference in isotherm pattern appears in Fig. 7. The corresponding velocity vectors in both the reference frame moving with the drop

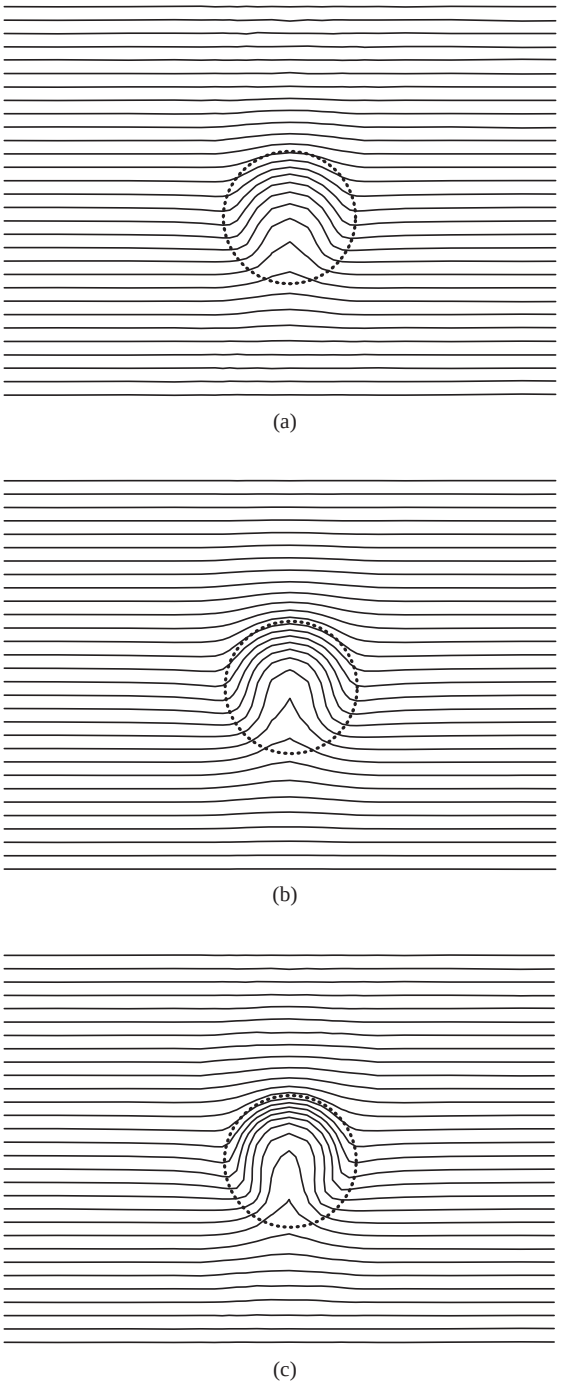

Fig. 7. Isotherms with a non-dimensional temperature increment 0.2 in the $x-z$ meridian plane for the drop radius (a) $a=0.259$ cm, (b) $a=0.326$ cm and (c) $a=0.377$ cm.

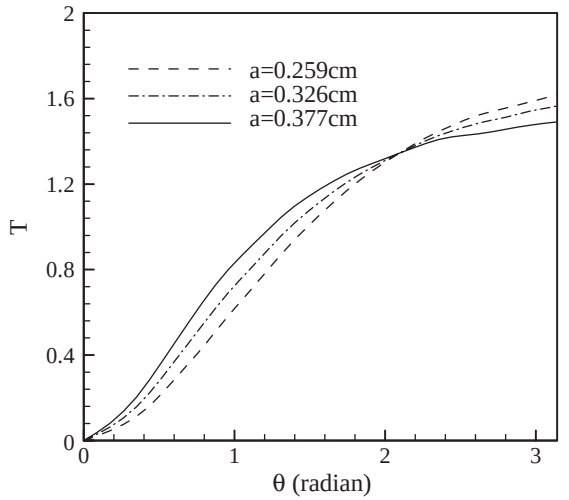

Fig. 8. Surface temperature distributions at different drop diameters.

and the inertial laboratory reference frame are shown in Figs. 11 and 12. To clearly exhibit the vectors, the patterns in Figs. 11 and 12 are drawn in selected coarse mesh points. It is seen that the vector magnitudes increase with the increase of the drop diameter, which is consistent with the results shown in Figs. 3 and 5.

5. Concluding remarks

Thermocapillary migration of a drop in a temperature gradient has been investigated numerically. The three-dimensional incompressible Naiver–Stokes equations and the energy equation are solved by use of a Galerkin finite-element method. The front tracking technique is employed to simulate the interface discontinuity. To simplify the present calculation, it is assumed that the drop keeps its spherical shape when the drop moves toward the high temperature region. This assumption is reasonable under the microgravity environment. Some typical cases, which have been investigated experimentally, are calculated using the present method. The calculated results are in good agreement with the experimental data, and demonstrate that the present method and code are capable of predicting the drop migration in a temperature gradient under the microgravity environment. From the comparison

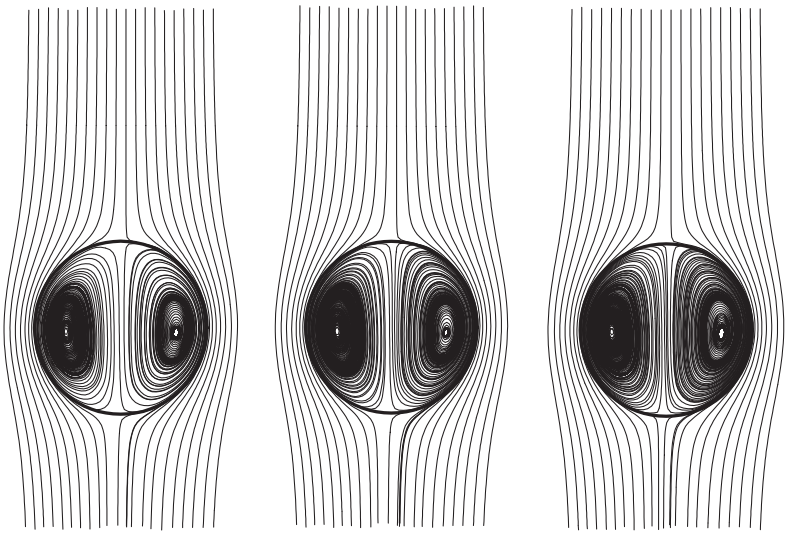

(a) (b) (c)

Fig. 9. Streamlines in a reference frame moving with the drop in the $x - z$ meridian plane for the drop radius (a) $a = 0.259$ cm, (b) $a = 0.326$ cm and (c) $a = 0.377$ cm.

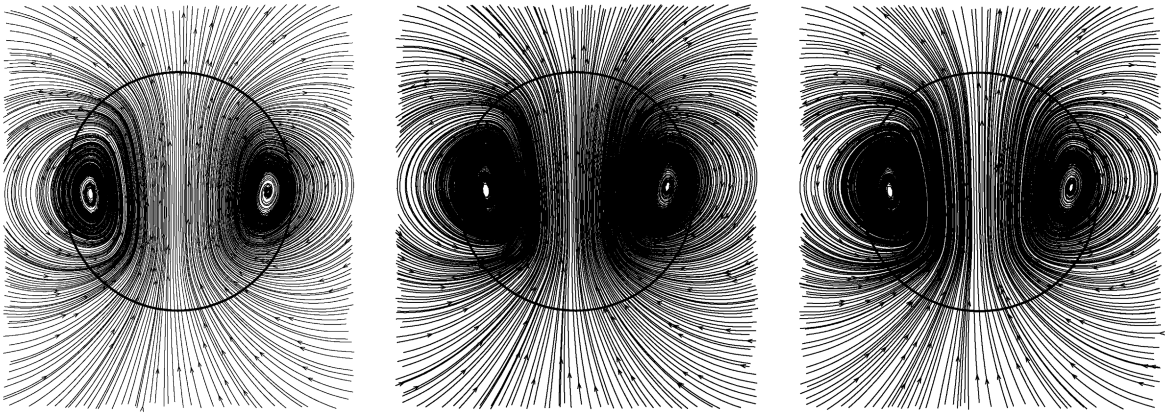

(a) (b) (c)

Fig. 10. Streamlines in an inertial laboratory reference frame in the $x - z$ meridian plane for the drop radius (a) $a = 0.259$ cm, (b) $a = 0.326$ cm and (c) $a = 0.377$ cm.

between the present results and that calculated by Geng et al. [14] using the two-dimensional flow equations, we can see that the two-dimensional flow assumption leads to the over-estimate of migration velocity significantly. This method can be extended to treat the three-dimensional flow with drop deformation, which is currently in the course of processing.

Acknowledgements

This work was supported by the National Science Fund for Distinguished Young Scholars (No. 10125210), the National Natural Science Foundation (No. 19789201), the Programme of the Hundred-Talent of CAS, and the Programme of the

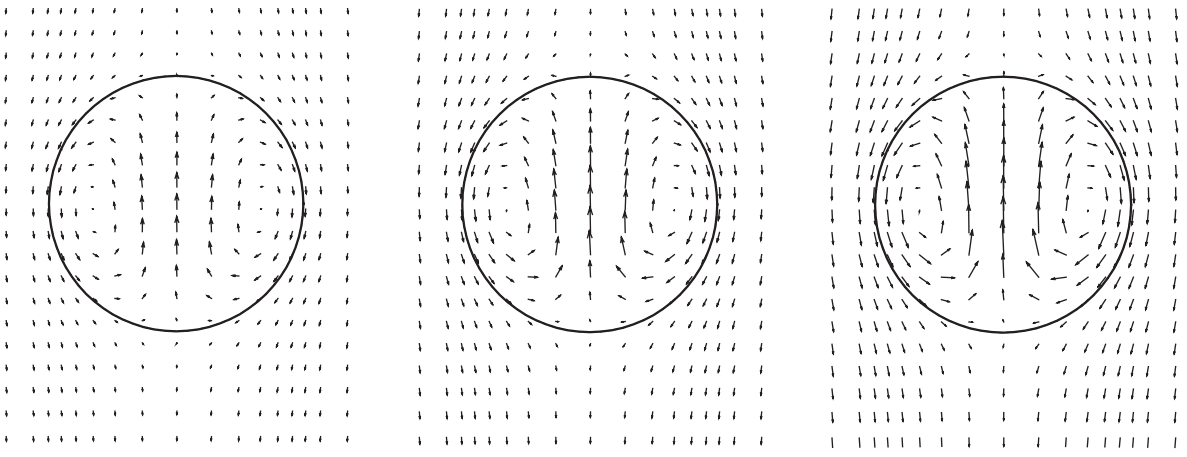

Fig. 11. Velocity vectors in a reference frame moving with the drop in the $x-z$ meridian plane for the drop radius (a) $a=0.259$ cm, (b) $a=0.326$ cm and (c) $a=0.377$ cm.

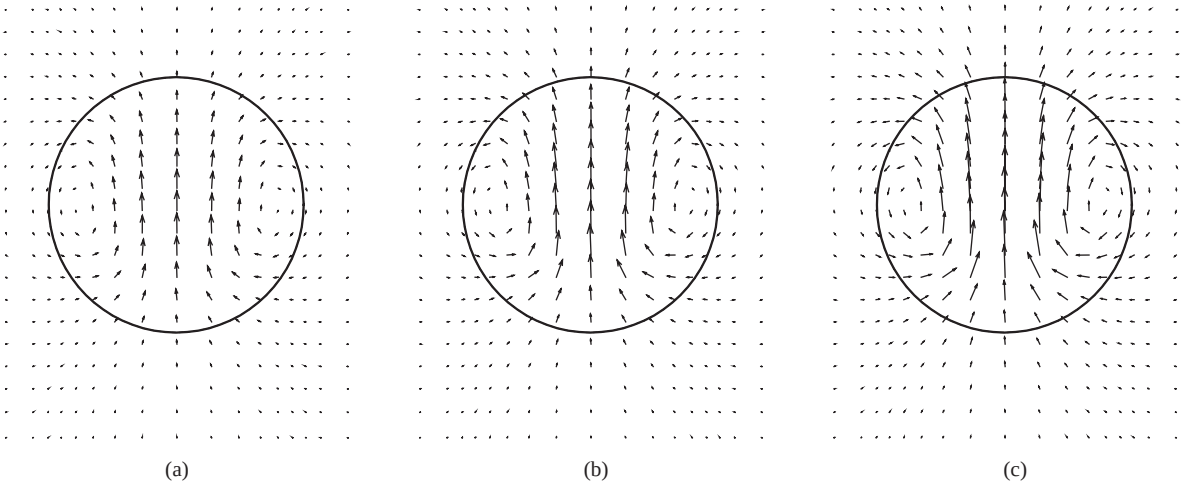

Fig. 12. Velocity vectors in an inertial laboratory reference frame in the $x-z$ meridian plane for the drop radius (a) $a=0.259$ cm, (b) $a=0.326$ cm and (c) $a=0.377$ cm.

Trans-Century Outstanding Young of National Ministry of Education (MOE).

References

[1] N.O. Young, J.S. Goldstein, M.J. Block, The motion of bubbles in a vertical temperature gradient, Journal of Fluid Mechanics 6 (1959) 350–356.

[2] B. Braum, C. Ikier, H. Klein, Thermocapillary migration of droplets in a binary mixture with miscibility gap during liquid, liquid separation under reduced gravity, Journal of Colloid Interface Science 159 (1993) 515–516.

[3] G. Wozniak, On the thermocapillary motion of droplets under reduced gravity, Journal of Colloid Interface Science 141 (1991) 245–254.

[4] J.C. Xie, H. Lin, J.H., Han, X.Q. Dong, W.R. Hu, A. Hirata, M. Sakurai, Experimental investigation on Marangoni drop

migration using drop shaft facility, International Journal of Heat and Mass Transfer 41 (1998) 2077–2081.
[5] M. Hahnel, V. Delitzer, H. Eckelmann, The motion of droplets in a vertical temperature gradient, Physics of Fluids 1 (1989) 1460–1466.
[6] M. Nallaui, R.S. Subramanian, Migration of methanol drops in a vertical temperature gradient in a silicone oil, Journal of Colloid Interface Science 157 (1993) 24–31.
[7] R. Balasubramaniam, R.S. Subramanian, Thermocapillary bubbles migration—thermal boundary layers for large Marangoni numbers, International Journal of Multiphase Flow 22 (1996) 593–612.
[8] R.S. Subramanian, Slow migration of a gas bubble in a thermal gradient, A.I.Ch.E. Journal 27 (1981) 646–653.
[9] R.S. Subramanian, Thermocapillary migration of bubbles and droplets, Advances in Space Research 3 (1983) 145–152.
[10] R. Balasubramaniam, R.S. Subramanian, The migration of a drop in a uniform temperature gradient at large Marangoni numbers, Physics of Fluids 12 (2000) 733–743.
[11] J.A. Szymczyk, G. Wozniak, J. Siekmann, On Marangoni bubble motion at higher Reynolds and Marangoni numbers under microgravity, Applied Microgravity Technics 1 (1987) 27–34.
[12] J.A. Szymczyk, J. Siekmann, Numerical calculation of the thermocapillary motion of a bubble under microgravity, Chemical Engineering Communications 69 (1988) 129.
[13] R. Balasubramaniam, J.E. Lavery, Numerical simulation of thermocapillary bubble migration under microgravity for large Reynolds and Marangoni numbers, Numerical Heat Transfer, Part A 16 (1989) 175–189.
[14] R.H. Geng, W.R. Hu, C. Ao, Asymmetric drop Marangoni migration of larger Reynolds numbers, Acta Astronautica 41 (1997) 757–762.
[15] H. Haj-Hariri, A. Nadim, A. Borhan, Effects of inertia on the thermocapillary velocity of a drop, Journal of Colloid and Interface Science 140 (1990) 277–286.
[16] H. Haj-Hariri, Q. Shi, A. Borhan, Thermocapillary motion of deformable drops at finite Reynolds and Marangoni numbers, Physics of Fluids 9 (1997) 845–855.
[17] S. Nas, Computational investigation of thermocapillary migration of bubbles and drops in zero gravity, Ph.D. Dissertation, University of Michigan, 1995.
[18] X. Ma, R. Balasubramaniam, R.S. Subramanian, Numerical simulation of thermocapillary drop motion with internal circulation, Numerical Heat Transfer, Part A 35 (1999) 291–309.
[19] A. Kovacs, M. Kawahara, A finite element scheme based on the velocity correction method for the solution of the time-dependent incompressible Navier–Stokes equations, International Journal of Numerical Methods in Fluids 13 (1991) 403–423.
[20] S.O. Unverdi, G. Tryggvason, A front-tracking method for viscous incompressible flows, Journal of Computational Physics 100 (1992) 25–37.
[21] G. Agresar, J.J. Linderman, G. Tryggvason, K.G. Powell, An adaptive, Cartesian, front-tracking method for the motion, deformation and adhesion of circulating cells, Journal of Computational Physics 143 (1998) 346–380.
[22] Y.X. Wang, X.Y. Lu, L.X. Zhuang, Finite element analysis of viscous flow past a rotating sphere, Journal of Hydrodynamics, Series B 13 (2001) 80–85.
[23] G.K. Batchelor, An Introduction to Fluid Dynamics, Cambridge University Press, Cambridge, MA, 1967, pp. 244–246.